The Utility of Torsion in Hot Workability Testing of Metallic Materials

E. EVANGELISTA - Dept. of Mechanics - Ancona University, I-60131 Ancona, Italy - H.J. MCQUEEN and N.D. RYAN, Mechanical Engineering - Concordia University, Montreal, H3G 1M8 Canada

Abstract

The hot torsion test has proven very versatile in determining high temperature ($>0.5\ T_m$) characteristics at constant strain rates of 10^{-3} to $10^{2}\ s^{-1}$. The stress-strain and strain hardening curves are suitable bases for constitutive equations giving temperature and strain rate dependencies. Critical points in the above curves in association with metallography clarify the progress of the restoration mechanism and the influence of solutes, precipitates and inclusions. The ductility is related to how the softening mechanisms delay the fracture mechanisms stemming from the alloy structure. The rate of static softening after hot deformation is determined by comparing the yield stress on reloading after an interval to that before it; many measurements for different times can be carried out on a single specimen by recrystallizing it between each stage in the torsion apparatus. The physical simulation of rolling schedules having many passes with declining temperature and rising strain rate is possible on computerized machines.

Riassunto

Le prove di torsione rappresentano un mezzo molto versatile per determinare il comportamento dei metalli ad alta temperatura a velocità di deformazione comprese tra 10^{-3} e $10^{2}\ s^{-1}$. Le curve sollecitazione-deformazione e incrudimento-sollecitazione costituiscono elementi per le equazioni costitutive che forniscono le relazioni con la temperatura e la velocità di deformazione. I punti critici delle curve e le osservazioni metallografiche indicano lo sviluppo dei meccanismi di ripristino e l'influenza su essi dei soluti, dei precipitati e delle inclusioni. La duttilità è correlata al modo in cui i meccanismi di addolcimento influenzano quelli della frattura che dipendono dalla evoluzione strutturale. La velocità dell'addolcimento statico che interviene dopo la deformazione a caldo è determinata confrontando lo snervamento che il provino manifesta riapplicando la sollecitazione dopo un intervallo di tempo. In tal modo possono essere effettuate molto misure sullo stesso campione ricristallizzandolo direttamente nella macchina di torsione. Il metodo consente infine la simulazione fisica, mediante computer, di cicli a molti passaggi che si eseguono con diminuzione di temperatura ed aumento della velocità di deformazione.

Introduction

In order to economically produce an optimum metal product by any of the industrial hot forming processes, it is imperative to have a comprehensive knowledge of its hot strength, ductility and microstructural evolution. Improvements in productivity and quality are essential for the viability of the metals industry in the face of invasive competition from ceramics and polymers. This is especially so for high temperature mechanical working which constitutes a primary stage for 80% of metal manufacturing.

The torsion test has proved its suitability for hot workability testing over the past 30 years [1-20]. Constant strain rates over a wide range are easily developed compared to tension or compression. Moreover, having no inherent instabilities, the strains in any process, e.g. extrusion ($\varepsilon = 3$-10), planetary rolling ($\varepsilon = 2$-5), continuous rolling total ($\varepsilon = 4$-5), can be matched and the precise influence of composition, cast structure, homogenization and heat treatment can be clarified. Several reviews are available which describe its methods, discuss it critically and compare it to other workability tests [2-4, 18-20]. In this paper, the capabilities for determining the main features of hot workability are covered: (1) dependencies of flow stress σ, microstructure and ductility ε_f on temperature T and strain rate, $\dot{\varepsilon}$ (2) mechanisms of deformation, restoration and fracture, and (3) multistage testing for static softening and physical simulations. The paper includes practical advice on how to carry out the various types of analyses stemming from torsion tests, providing qualifications regarding certain interpretations. Since the objective is to clarify the capabilities of the torsion test, explanations of the physical metallurgy are not given in their entirety; they can be found in the original publications [5-18,21-47]. Illustrations are drawn primarily from the authors' wide experience with aluminium alloys [7,8,25-40] and with carbon, HSLA [41,42], tool [42] and stainless steels [9-17,44-47].

The test machine and specimen geometry

The apparatus can most simply be thought of as a lathe on which the tail stock is replaced with a rigid

clamp which also serves as the torque transducer. The cutting tool holder is replaced by a furnace most commonly of the radiant or induction type which can change temperature quickly in response to programmed schedules or to compensate for deformation heating. If an electric motor and gears are used the other necessary components are (1) a clutch so that the specimen is engaged only after it is at temperature, and for the duration related to the desired strain, and (2) a fly wheel which ensures that the speed remains constant when the specimen is engaged [47-49]. The alternative drive is an hydraulic motor controlled by servo valves (Fig. 1), with capabilities similar to those in current tension-compression machines [18]. Programming of the latter machine is quite easy so that strain rate changes from stage to stage pose no difficulty; a problem compared to the electric motor, however, is lower rotational speeds. For the electro-mechanical drive, strain rate changes require manual gear shifts during intervals of sufficient duration. However, there are some motors available which can vary speeds electronically. The strain is measured from the rotation of the drive system; rotary potentiometers or optical slit encoders have been employed. The difficulty is in combining accuracy with high revolutions, sometimes as high as 50.

The most commonly used specimens have a gauge length L of 20-30 mm and a diameter 2r of 6-10 mm. A larger 2r/L ratio provides for a higher equivalent surface strain rate:

$$\dot{\varepsilon} = (2\ \pi\ r/\sqrt{3}\ L)\ \text{(revolutions/sec)} \qquad (1)$$

The equivalent strain, ε, and equivalent stress, σ, below are derived by von Mises' theory (shear strain x $1/\sqrt{3}$; shear stress x $\sqrt{3}$). A stubbier specimen improves T constancy since it facilitates conduction of heat generated by the deformational work. However, as the ratio declines toward unity there are more problems with deformation extending into the shoulders thus reducing the strain accuracy which is measured externally. Solid specimen are commonly used since they are more easily produced than tubes and do not suffer buckling as the wall thickness is reduced. The gradient in stress is compensated mathematically taking account of the hardening effects on the torque Γ of the strain gradient ($n'' = d\Gamma/d\varepsilon$) and of the strain rate gradient ($m = d\Gamma/d\dot{\varepsilon}$) (1):

$$\sigma = (\sqrt{3}\ \Gamma/2\ \pi\ r^3)\ (3 + m + n'') \qquad (2)$$

the value of m is determined for each temperature from the slope of torque Γ versus ε curves. The value of n'' is taken as zero which is true for the peak stress and the steady state regime as explained later. The use of $n'' = 0$ does engender small errors in other sections of the σ-ε curves.

The specimen temperature may be controlled by a thermocouple pressed against the centre of the gauge section so that it does not impede rotation. Alternately, the temperature may be measured by thermocouples inserted down the axis in both shoulders close to the gauge section; this permits balancing of the temperature profile by moving the furnace along the axis [48]. In either case, care must be taken before any test to ensure that the temperature is uniform along the entire gauge section; insofar as this is not the case, strain concentrates where T is high and vitiates the external measurement of ε and $\dot{\varepsilon}$. Such true strain is reported as a pure number as distinct from % reduction in compression, rolling or tensile neck area, or % elongation in tension, measures which can be converted to true strain.

Flow curves and strain-hardening-stress plots

The σ-ε and strain hardening-stress curves Θ-σ, ($\Theta = d\sigma/d\varepsilon$), are illustrated in Figs. 2 and 3. Aluminium and its simpler alloys generally have curves that exhibit monotonic hardening to a steady state regime σ_s (which may gradually decline due to deformational heating at high $\dot{\varepsilon}$) [5-8,24-31]. The steady state plateau results from dynamic recovery providing a balance of dislocation generation and

annhilation to give subgrains of constant size d_s and wall character. Such behaviour is also found for bcc alloys of Fe, Ti, Zr and refractory metals. The Θ-σ plots decline in two linear segments which reach the saturation stress $\sigma_s^* = \sigma_s$. The curved segment coincides with subgrain formation which gradually spreads from the grain boundary region to the grain centre.

The σ-ε curves for austenitic stainless steels [9-17,44-47,50,51] which are representative of Cu, Ni and Fe [5-8,18,21,43,50] show the characteristics of dynamic recrystallization (DRX). The Θ-σ curve shows a downward inflection in its lower segment which indicates nucleation of DRX [9-15,45]. The extrapolated lower segment gives σ_s^* which would result from DRV alone (if DRX did not occur). The experimental curve reaches $\Theta = 0$ at σ_p, ε_p the peak of the σ-ε curve. The flow softening (Figure 3) reflects the progress of the first wave of DRX which is complete at the inception of the steady state at ε_s', σ_s'. DRX occurs repeatedly throughout the steady state regime to lower the average dislocation density (d_s' is larger than d_p). The recrystallized grain size is also maintained constant at D_s which depends only on T and $\dot{\varepsilon}$.

The flow curves of alloys undergoing microstructural changes are more complicated. In solution treated alloys, mainly Al alloys (possibly microalloyed steels), dynamic precipitation may occur and give rise to a high stress peak which rapidly declines as the particles coarsen (Figure 4) [30,35-39]. If fracture does not intervene (GB cracking at the high stresses), the curve declines to an equilibrium value which is monotonically attained by pre-aged specimens with coarse particles. Pre-aged specimens are often only slightly stronger than the pure metal because of the low solute level and have similar T and $\dot{\varepsilon}$ dependence.

The flow curves in torsion do not provide as accurate values of high temperature yield stress σ_o as do compression or tension because of the simplification in use of Eqn 1. While this is significant in some investigations it is not crucial in modelling. The traditional formulae require k_p which is the average flow stress for the strain in an individual pass or stage. In finite element analysis, an equation representing the flow curve is wanted. While many are available, a suitable one has recently been derived for either torsion or compression employing reduced σ/σ_p (or σ/σ_s) and $\varepsilon/\varepsilon_p$ (or $\varepsilon/\varepsilon_s$) [52,53].

$$(\sigma/\sigma_p) = [(\varepsilon/\varepsilon_p)\ \exp\ (1 - \varepsilon/\varepsilon_p)]^c \tag{3}$$

The values of c are determined for each flow curve but analysis indicates that a single material constant may be a suitable approximation. For DRX material the curve to the peak is sufficient for most operations since strains seldom exceed 0.4. However, for extrusion and planetary rolling, the entire flow curve must be used [45].

Constitutive equations

The dependence of flow stress of T and ε is usually obtained for either the steady state stress σ_s or the peak stress σ_p (Fig. 5). The common forms suitable for the high stresses of hot working are [5,21,42]:

$$A\ (\sinh\ \alpha\sigma)^n = \dot{\varepsilon}\ \exp\ (Q/RT) = Z \tag{4}$$

$$\text{or}\ A''\ \exp\ (\beta\sigma) = \dot{\varepsilon}\ \exp\ (Q/RT) = Z \tag{5}$$

where A, A″, α, n and $\beta = \alpha n$ are material constants. Z is the Zener-Hollomon parameter and includes both the experimental control variables $\dot{\varepsilon}$ and T. The activation energy Q is usually designated Q_{HW} for σ_s in DRV alloys [5,24-31] or for σ_p in DRX alloys [9-17,43,44-47]. A plot of Z against a stress function draws the data for all conditions into a single line which facilitates interpolation (Fig. 6). For σ_s' in DRW alloys, Q is labelled Q_{DRX} since it relates to completion of the first wave [9-11]. It is lower than Q_{HW} since

the flow softening is greater at high Z than at low (a lower range of σ_s variation). It is utilized in Elfmark's prediction of hot ductility [4].

In Al alloys with low solute levels which includes those with precipitates over-aged so as to have little effect on dislocation motion, the activation energies are similar to pure aluminium ($\approx$150 KJ/mole) [23,24,27,30]. However, Q_{HW} rises with solute content such as levels of Mg exceeding 2% [24,31,34]. For alloys in the solution treated condition, dynamic ageing at low T produces extraordinarily high σ_p, whereas at high T the precipitation is less and coarsening more rapid. This results in a Q value which is normal at high T but is about twice normal at low T [30,35-40]. Alloys with stable dispersoids usually have high values of Q [25,28-30]. Sheppard has compiled constants for a wide selection of alloys and has also shown that torsion derived constants are suitable for predicting extrusion pressures and calculation of limit diagrams [54-57]. For carbon steel, Q_{HW} is about 300 KJ/mol and increases in HSLA, or tool steels (possibly different values at high and low T because of precipitation at low T) [41,42]. The Q_{HW} constants have been collected for 70 alloys covering types 301, 304, 316 and 317 steels [9,10,16]. These were found to increase linearly with solute content form 400 to 500 KJ/mol.

Hot ductility

In torsion the fracture strain ε_f is notably high, but as shown in Fig. 7, exhibits a wide range of variation with T and ε and with the alloy composition and structure (as-cast or as-worked) [4-6,8-10,12,15,17,24,25,42,44,47,50,51,58-61]. Microscopic observation shows that the high temperature fracture mode consists of crack initiation at triple junctions and propagation along grain boundaries (GB) (Fig. 8) [5,6,8,39,42,60-64]. The large ε_f provide an opportunity to see that DRV within grains delays the initiation and that DRX diminishes the propagation by separating GB from the fissures. The influence of inclusions, constituent particles and massive second phase in enhancement of cracking and retardation of restoration have been observed [63,64]. Fractography has not been of much use because the fracture surfaces rub together.

The torsion test provides a more accurate measure of inherent ductility than either tension which is subject to necking or compression which is subject to barrelling due to friction with the platens. In these last two tests, failure is related to specific instabilities which differ from those found in hot forming processes. The micro mechanisms of fracture are the same in all tests and processes and are speeded up by local tensile stresses which can be specified in terms of the local mean stress (σ_{mn} which is the average of the three orthogonal principal stresses) [61,63]. Due to the neck induced hoop stress, σ_{mn} is very high in tension enhancing decohesion. In forging, rolling, or extrusion, σ_{mn} is generally negative inhibiting crack growth but at the surface, such as the edge in rolling or the die land in extrusion (high friction), σ_{mn} is locally positive accelerating fissure propagation. In torsion, σ_{mn} is zero but there is one tensile component at 45° to the axis which assists some pores to grow but not the principal ones developing on the transverse shear plane. The compressive component also at 45° to the axis is not able to weld shut those same pores. The net effect is that the ductility is much higher than the localized unstable ductility in forming processes (which only arise at some high total strain). Torsion ranks different alloys, or different microstructures for a given alloy, in the order of their inherent ductilities. Because it stretches out the magnitude at higher strains, Young and Sherby [65] have proposed a lower correlation of ductility in torsion to that in tension, the power being unity up to $\varepsilon = 1$ and one half at higher strains.

Microstructures

The preferable section for examination of torsion specimens is a tangential or chord plane which

exposes the original grains as elongated fibres which become thinner and closer to normal to the axis as ε increases (Fig. 9) [32,33,66-68]. It should be as close as possible to the surface because ε and $\dot{\varepsilon}$ decrease with depth; however, it must be wide enough to be a representative structure and deep enough to be below surface grooving. This section has many similarities to the thickness plane parallel to the rolling direction. If dynamic or static recrystallization takes place, it is quite noticeable in this plane. However, its occurence should be checked on the two perpendicular sections. In the longitudinal plane, the grains appear thin at the surface but gradually thicken to the initial dimension at the axis. If DRX or SRX has occurred, it is usually in an outer annulus. In the transverse plane normal to the axis, the deformed grains retain their original dimensions unless there has been recrystallization. With the DRX or SRX, the grains should be equiaxed in all three planes (Fig. 10) [34,69]. At high strains, when grain thickness is almost the same as the subgrain diameter, then equiaxed subgrains could dominate the tangential and longitudinal sections but the transverse would show the original grain dimensions [32,33,66-68].

Foils for transmission electron microscopy are best taken tangentially at a known radius [9-11,13-15,20,29,33,34,66-69]. This is achieved by cutting the specimen with the axis parallel to the plane of a diamond wafering blade. The first slice should be from the surface to a depth of 0.5 mm; a second slice of equal thickness may then be cut. It is usually possible to cut 3 sets of slices around the axis at 120°; each may be long enough to give several discs in the axial direction. The slices are then smoothed and thinned by fine grinding and by chemical polishing. The jet discing should be along the centreline of the slices so that the thinned section is normal to a radius. There is not usually a need to examine other sections if there has been adquate optical microscopy. The latter is extremely important in providing a microscopic understanding while the TEM gives information on the presence, dimensions and character of substructure to characterize DRV (Fig. 11) and to distinguish between DRX and SRX [9,14,29,33,34,67-69]. In checking for DRX it is important to show that the grain size delineated by Selected Area Diffraction, SAD, in TEM corresponds to those in optical microscopy. SAD is important in confirming the misorientation across boundaries. Tilting the foil can also characterize a boundary by bringing the dislocations into contrast. Statistical distributions of boundary misorientations may be necessary to characterize the microstructure especially if the original boundaries are highly serrated and close together [59,68].

Scanning Electron Microscopy, SEM, in channelling contrast mode is a very effective tool since it gives a large field of view and does not depend on etching (70). It is able to distinguish SRX grains from either initial or DRX grains which are noticeably mottled by substructure (Fig. 12) [15]. It is possible to use the contrast quantitatively to determine orientations. SEM does not reveal the character of the boundaries and may not resolve boundaries of low misorientation as can be seen in TEM. Thus the TEM subgrain size is likely to be lower than that from SEM. Optical microscopy relying on etching or the formation of an oriented oxide film from polarized optical microscopy (POM) is likely to give larger subgrains due to difficulties of etching or of nucleating separate oxide patches if the misorientation is low [67,68].

The torsion test is as capable of producing observable microstructures as other techniques; the geometry of examination varies with the stress axis and the need to surmount inhomogeneities such as barrelling or necking. However, another important feature for observing the worked microstructure is the ease of extricating the specimen from the furnace and quenching it. In this respect, torsion is as good as tension for "in situ" quenching (compression anvils get in the way) and as simple for extraction and external quenching as compression if the rotating grip is simply a slot and the fixed grip (threaded) retracts longitudinally. Very fast quenching can be attained by water spraying the specimen without removing it from the high frequency induction coil.

One of the most important features to observe in the as-worked, is the substructure which is present after both DRV alone and DRX as long as SRX has not occurred. The important features are the shape, size, perfection of the subgrains and the dislocation arrangements and misorientations of the SGB

[9,11,13-15,28,29,31,45,67-69]. The constants, a, b, c, and e can then be determined for the relationships relating d_s to T, ε and σ (Fig. 13):

$$d_s^{-1} = a + b \log Z \tag{6}$$

$$\sigma = c + e\ d_s^{-1} \tag{7}$$

The substructures may be altered in density during slow cooling after the deformation by static recovery. If the specimen appears to have undergone SRX optically, the retention of substructure indicates that SRX is incomplete.

In specimens with equiaxed grains, the size may be measured to determine the following equations giving the dependence on T, $\dot{\varepsilon}$ and σ:

$$D_s^{-1} = a' + b' \log Z \tag{8}$$

$$\sigma' = c' + e' D_s^{-p} \tag{9}$$

where a′, b′, c′, e′ and p ($\approx$0.8) are constants which have different values for SRX and DRX [9-15]. Which of these two has occurred can be ascertained by checking for substructure. For elongated grains, the thickness can be sampled in various regions and the strain estimated to survey uniformity. The grain boundaries usually become serrated, the wave length being approximately equal to the subgrain size. When the elongated grains become as thin as twice the subgrain diameter they usually are difficult to distinguish because of the irregular boundaries and pinching-off (perforating in 3 dimensions) where opposing serrations impinge [32,67,68]. In cases of doubt, the grain boundaries should be followed as a function of strain to see whether they persist; tests could be performed with different initial grain sizes. It is important to know the initial grain size and to maintain it constant in a series of tests unless varied purposely to determine effects on the flow curve and microstructural evolution. It has a strong effect on the rate of DRX because the new grains frequently form at the pre-existing GB [5-7].

Another important microstructural change is the development of a preferred orientation which has been measured in Al as a function of strain. Fig. 14 shows the texture that develops at intermediate strains of 5-10 which agrees with the common theories of polycrystalline slip constraints and crystal rotations [33,66,68]. At high strains (ε=20-60), a different texture develops due to relaxation of the constraints with the formation of thin grains with parallel sides. It also leads to about 20% softening which must be distinguished from decline in flow stress due to DRX which takes place at much lower strains [59,66,68]. Copper initially develops the same texture as Al but as DRX takes place, the texture does not strengthen [71,72]. Because the grains remain roughly equiaxed, the high strain Al texture never develops. Stainless steel in expected to behave like Cu [71,73]. It should be noted that the softening due to texture has little effect on the other microstructural features, notably, the subgrain size and wall misorientations remain unchanged. Of course as the GB became parallel, closer together and more serrated, it becomes more difficult to distinguish the elongated grains as explained earlier.

The texture development depends entirely on the mode of deformation so that the texture in torsion is not an immediate guide to that in rolling [33,68-73] or wire drawing. However, since they can all be derived from the same slip and constraint theories, a change in texture in one mode due to changes in mechanism would signal an equivalent change in another mode; in Al, there is no such change, whereas with Cu and stainless steel there is. However, because the high $\dot{\varepsilon}$ in rolling retards DRX and the usual strains are insufficient to go beyond the intermediate texture, Al, Cu, and stainless steels generally have the same rolling deformation and recrystallization textures [64]. At low strains (ε<2) with isotropic material, the substructures and flow stresses developed in torsion, tension and compression are similar (the von Mises' theory provides a suitable conversion for torsion). However, the texture development in torsion leads to softening, whereas those in tension and compression lead to hardening, thus the flow stresses diverge unless Taylor factor analysis is used to convert all values to a theoretical isotropic

property [66,72]. Because of limited strain in the latter two tests, the intense textures equivalent to the final torsion texture cannot develop.

Static recrystallization following hot working stages

In many hot working processes, the metal is not cooled rapidly after deformation so that some static recrystallization (SRX) takes place [6,8,24,41,42,74,75]. This most commonly occurs in multistage operations such as rolling or closed die forging with considerable effect on the strength in the following stage. However, in a high-speed continuous strip mill the times between stands is so short that in some alloys there is no SRX. At the end of processing, the rate of cooling affects static softening so may be controlled to induce desired properties in the product, e.g. the periphery of extrusions may undergo SRX. As a result, knowledge of the rate of recrystallization is very useful. The determination could employ metallography, or other techniques, used in annealing after cold working. The parameters to be considered are not only the temperature after deformation but also the strain, strain rate and temperature during deformation which all affect the stored strain energy. A common situation is for the workpiece to be held so that the deformation temperature becomes the one effective during SRX. Holding at temperature after forming leads to more rapid SRX than quenching and then annealing because the reheating enhances static recovery, SRV, which reduces the strain energy during SRX [24.31]. Torsion testing is a suitable as other tests although there is a blend of limitations and advantages in mechanical measurements of SRX as explained later.

A very convenient technique to measure the softening after an interval of holding at temperature is to reload the specimen in the original mode [6,8,75]: Al alloys [24,31,35], C-HSLA steels [41,42,74] and stainless steels [17,42,44,74,76,77]. The fractional softening, FS, at time t is given by:

$$FS(t) = (\sigma_r - \sigma_o)/[\sigma_m - \sigma_o) \quad (10)$$

where σ_m is the stress before unloading, σ_r that on reloading and σ_o the yield stress all at the same T and $\dot{\varepsilon}$ (Figure 15). In the simplest form, for each time, there is a separate two-stage or interrupted test which may be carried out by compression, tension or torsion. Because of the very high strains available compared to other modes, the torsion test may be adapted to give half a dozen softening measurements across the series of time spans desired [76,77]. However, between each test, it is necessary to restore completely recrystallized grains of the original size by giving the specimen a large predetermined strain and holding period between each measuring cycle. With one torsion specimen and programmed test, data can be derived equivalent to half a dozen compression or tension tests with time-consuming individual set-ups. The fractional softening may be plotted as a function of holding time to provide the traditional S-curve [7,31,76,77]. The data can also be subjected to Avrami analysis according to the following equation:

$$FS = 1 - \exp(-c\ t^k) \quad (11)$$

The time exponent k is lower than for microscopic studies since FS includes a recovery component. The temperature dependence can also be shown to obey an Arrhenius relation:

$$FS'(T) = B' \exp(-Q'_{SRX}/RT) \quad (12)$$

$$FS''(T) = B'' \exp(-Q''_{SRX}/RT) \quad (13)$$

where B' and Q''_{SRX} are constants referring to varying T of deformation and holding; different values of B'' and Q''_{SRX} would be found for constant T deformation but varying T of SRX. From these equations

one may calculate the amount of crystallization for intervals of various times and temperatures.

In multistage operations, the important concern is not just the initial stress on reloading but the change in the flow stress across the entire second stage in order to find the average pass stress for calculating separating force and torque. This is physically modelled in the two-stage test. It has also been of interest to model the effect of a fixed mixture of SRX and pre-deformed grains entering the second pass on the recrystallization in the interval (the second) after that pass by measuring the FS by means of a third deformation [75]. In the torsion test it is possible to do many identical stages with similar (or varying) times [17,24,31,34,41,42,44,74,75]. The result is that if softening is 100% then the succeeding curves are identical to the first. If the SRX is incomplete, the softening gradually builds up in succeeding intervals because regions subjected to two or more stages recrystallize faster than those with one stage; however a stable softening level is finally established. These multistage isothermal curves are not simulations of industrial rolling in which T declines from pass to pass as described later under physical modelling. A limitation of "mechanical metallography" is that it measures the combined effect of SRV and SRX; however, these can, be separated if the entire softening curve is determined [75]. It is also possible to calibrate the relation of FS to fraction SRX by metallography [76-80]. Determination of softening by torsion is affected by the gradient in strain energy (both ε and $\dot{\varepsilon}$ decreases) with limitation of SRX to an outer annulus so that the normal correction factor is not precisely valid. Nevertheless, the technique works satisfactorily as checked by metallography because of the dominating influence of the outer stress which is multiplied by the radius cubed.

Physical simulation of multistage rolling schedules

As discussed in the previous section, it is possible to establish equations through which the amount of recrystallization in an interval can be calculated [73,74]. From that, it is possible to estimate the flow curve in the succeeding pass by assuming the SRX grains behave as the original grains in the first pass and the retained deformed material strengthens on beyond the s_M in continuance of the first flow curve. There is the further assumption of uniform distribution of, and equal strain in, both types of regions with adherence to the law of mixtures. In addition, the decline in T makes the calculations more complex. A more accurate alternative is the physical simulation of the process by means of programmed testing [74-80].

In most rolling schedules, a significant feature is the declining temperature profile which arises from cooling by either the rolls or the atmosphere between passes. The specimen temperature can be controlled according to the industrial profile in conjunction with the schedule of pass strains and delays which are matched to the mill [76-80]. Fig. 16 exhibits a series of passes simulating a cross-country bar mill which is marked by intervals of about 20 s. The diagrams show strain rates 0.1, 1 and rising 0.1-2 s^{-1} (selected because of limitations on the machine speed). Simulations of Al rolling schedules have been carried out by Vaughan [81] and by Farag and Sellars [82]. The fractional softening (the drop between the individual pass curves) requires a special mode of calculation because the reloading curve is raised relative to the unloading by the T decrease during the arrest [78-83]. FS diminishes as T declines so that part of the augmenting rise in pass flow stress is due to the increasing proportion of worked material being carried over [74,78-80]. It should be noted that the static restoration between passes also increases the ductility [8,42,44,78]. The validity of such simulations have been confirmed by comparing roll separating forces calculated from the torsion data with the measured forces in mill trials. In addition, the microstructures produced in torsion at the end of each pass have been found to agree with those from the mill [2,74,75].

Torsion simulation have been used to optimize rolling schedules for both production and experimental alloys [2,74,75]. These have proven particularly valuable for controlled rolling of

microalloyed steel where schedules were changed from those for carbon steel due to the former's greater hot strength. Moreover, the schedules provide a long delay after break-down to lower the temperature before the finishing passes. The microalloy solute and precipitates inhibit recrystallization between these passes to ensure a very fine grain size during a final SRX [41,42,74,75]. The torsion test can include the final cooling to bring about transformation to ferrite for a check on grain refinement; the ability to determine mechanical properties is discussed next. Other types of thermomechanical processing are looked at later.

Product properties

Determination of the final product properties is the fourth of the major goals of hot workability testing [82]. They may, to some degree, be inferred from the microstructures developed in the course of the entire process [79-81]. Nevertheless, it is valuable to measure them not only for their own utility but also as a means of confirming the microstructural analysis. A rapid and suitable means is hardness tests on the surface of the torsion specimens (Fig. 17) [82]. This measures the outer fibre properties in an isotropic manner, independent of the crystallographic or fibre orientation. Because of surface oxidation or micro-fissuring it may be advisable to do the tests on a ground flat similar to that used for optical metallography. It is also possible to take microhardness readings as a function of radius in longitudinal or transverse sections and hence find values for a greater variety of ε and $\dot{\varepsilon}$. Both testing configurations could be used in conjunction with static recrystallization which has occurred only in an outer annulus.

Tension and impact testing cannot reasonably be performed on solid torsion specimens because of the variation in microstructure from surface to centre. On the basis that the superior properties of the outer fibre might have a strong influence, tensile tests showed that the behaviour varied weakly in the sense expected [83]. Tension or compression tests on tubular samples might be satisfactory; however, machining out the centre after hot torsion poses difficulties because of the damage induced [33]. Cold torsion testing can measure the proof stress and strain hardening rate effectively because of the preponderant influence of the outer fibres [59]. The ductility resulting from different hot working conditions could be compared but the direction of rotation should be related to that in the hot test. Cold torsion results might be inaccurate if a thin peripheral layer has statically recrystallized becoming weaker than the core. When torsional strain exceeds 3, strong textures develop and would affect the cold strength making it difficult to compare properties with compression or rolling. However, cold torsion has been used to confirm that hot strength changes are due texture development and not to change in mechanism [59].

Thermomechanical processing

Thermomechanical processing (TMP) is the combination of thermal and mechanical effects to attain desired microstructure and properties [86,87]. An example of this would be the production of a structure capable of superplastic deformation. Alloys of Al-Li-Cu-Mg (AA8090) were deformed to a strain of 2 at $0.1\ s^{-1}$ and 300°C in order to develop a fine subgrain structure stabilized by precipitates [88,89]. During a hold of 300 s, some recovery takes place as the temperature is raised to 450°C. Straining is then continued at rates of 10^{-2} to $10^{-4}\ s^{-1}$. Superplastic deformation is confirmed by the strain rate sensitivity $m \approx 0.4$. Elevated elongation cannot be checked in torsion since high strains are often exceeded by DRV and DRX assisted dislocation deformation. The microstructure has also changed with the subgrain misorientation increasing to over 10° compared to 1° at the end of the initial processing.

The hot torsion testing of Al-0.65 Fe conductor wire has measured the effects of isothermal straining on flow stress and substructure in comparison to industrial processing [25,26,29,86,87]. The torsion machine could simulate the industrial schedule which consists of 13 passes with temperature declining from 500 to 180°C to produce a final strain of 4.3. This is followed by rapid cooling to room temperature to retain the substructure. The wire drawing could be matched by 12 equal passes for an additional strain of. 2.6. The test would show the final strength and, through incorporation of the final recovery anneal, measure the delivered strength. The torsion simulation could be used to optimize the process in terms of pass strains and temperature profile.

The press heat treatment of Al alloys has been examined only slightly by torsion testing [30,57,86,87]. The first aspect is the state of solution or of precipitation, including size and distribution, and the effects it has on the flow stress and the extrusion pressure. Torsion tests have shown that the solution treated material has a much higher peak stress (followed by softening) compared to material which has been cooled in a controlled way or pre-aged to produce particles of a size large enough to have a little effect on dislocations [30,35-40]. The second aspect is to find the conditions under which the particles redissolve by programming the torsion test to produce the extrusion strain while raising the temperature as in the extrusion press. This sequence would guide optimization of the preheat treatment and the billet temperature to give lower break-through pressures and ensure complete solution in preparation for quenching. The cooling cycle, including the delay between die and air jet, can also be simulated to find out the critical condition for full hardening as measured by hardness. In addition, the influence of particles and segregates left by homogenization, cooling and preheating rate on high temperature tearing can be determined under various conditions of billet temperature, ram speed (strain rate) and simulated deformation heating. Unfortunately, it is not possible to simulate the gradients of strain rate and temperature in the extrusion zone which are particularly severe near the boundary with the dead metal zone [54-57].

Conclusions

As illustrated in this paper, drawn from a considerable volume of research on steels and aluminium, the torsion test is capable of providing results on the complete range of characteristics related to hot workability. The most important are the flow stress and ductility dependencies on temperature and strain rate and the microstructural evolution during and after the deformation which leads to the product properties. The gradient of strain and strain rate in solid torsion bars can be resolved by plasticity analysis up to strains of about three; however, at greater strains, the development of a strong texture (especially when dynamic recovery is the sole mechanism) requires Taylor analysis. Suitable microstructural analysis by optical and electron microscopy are preferentially, but not exclusively, performed on tangential sections. Static restoration is successfully measured by two-stage testing; however, the presence of a stronger core beneath a thin, soft periphery could give misleading results. The product properties are successfully measured by hardness or cold torsion. The greatest advantage of the torsion mode is its capability to test to high strains which gives a significant advantage over other techniques in physical simulation of multi-stage processing. While the emphasis has been on industrial applications, torsional straining also permits examination of dislocation substructures, restoration mechanism and grain boundary impingement at ultra-high strains.

Acknowledgments

The background research was financially supported by the Natural Science and Engineering

Research Council of Canada and by the National Research Council (CNR) of Italy. Funding from the latter has made the collaboration possible.

References

[1] Rossard, C. Metaux, Corrosion, Industrie 35, (1960), 102-115, 140-153, 190-205.
[2] Rossard, C. and P. Blain *Flat Rolled Products III.* Gordon and Breech, New York. 1962, pp. 3-28.
[3] McQueen, H.J. and J.J. Jonas. *Metal Forming.* Plenum Press, London. 1971, pp. 393-428.
[4] Elfmark, J. Czech. J. Phys. B35 (1985), 260-274.
[5] Sellars, C.M. and W.J. McG. Tegart. Int. Metall. Rev. 17. (1972), 1-24.
[6] McQueen, H.J. and J.J. Jonas. In R.J. Arsenault (Ed.), *Treatise on Materials Science and Technology.* Academic Press, New York. 1975, vol. 6, pp. 393-493.
[7] McQueen, H.J., and J.J. Jonas. J. Appl. Metal-Work. 3 (1984), 233-241.
[8] McQueen, H.J., and J.J. Jonas. J. Appl. Metal-Work. 3 (1985), 410-420.
[9] Ryan, N.D., and H.J. McQueen. J. Mat. Proc. Tech. 21 (1990), 177-199.
[10] Ryan, N.D., and H.J. McQueen. High Temp. Tech. 8 (1990) 27-44, 185-200.
[11] Ryan, N.D., and H.J. McQueen. Can. Met. Q., 29 (1990) 147-152.
[12] Ryan, N.D., and H.J. McQueen. In S. Blecic (Ed.), *Int. Symp. on Plasticity and Resistance to Metal Deformation.* Ferrous Metall. Institute, Niksic, Yugoslavia, 1986, pp. 11-26.
[13] McQueen, H.J., N.D. Ryan and E. Evangelista. Mat. Sci. Eng., 10 (1986), 259-272.
[14] Ryan, N.D., H.J. McQueen and E. Evangelista. In N. Hansen et al. (Eds.), *Annealing Processes, Recovery, Recrystallization and Grain Growth.* Roskilde. 1986, pp. 527-534.
[15] Evangelista, E., N.D. Ryan and H.J. McQueen. Metallurgical Sci. Tech., 5 (1987), 50-58.
[16] McQueen, H.J. and N.D. Ryan. *Stainless Steels '87.* Inst. of Metals, London, 1987, 498-507.
[17] Ryan, N.D. and H.J. McQueen. In R.A. Lula (Ed.), *New Development in Stainless Steel Technology.* ASM, Metals Park. 1985, pp. 293-304.
[18] Fulop, S., K.C. Cadien, M.J. Luton and H.J. McQueen. J. Test. Eval. 5 (1981) 419-426.
[19] Luton, M.J. In G.A. Dieter (Ed.), *Workability Testing Techniques.* ASM, Metals Park. 1984, pp. 95-133.
[20] Semiatin, S.E., G.D. Lahoti and J.J. Jonas. *Metals Handbook.* ASM, Metals Park. 1985, vol. 9a, pp. 154-184.
[21] McQueen, H.J. and D.L. Bourell. In A.K. Sachdev et al. (Eds.), *Inter-Relationship of Metallurgical Structure and Formability.* AIME, Warrendale. 1987, pp. 341-368.
[22] McQueen, H.J. and E. Evangelista. Czech. J. Phys., B38, (1988) 359-372.
[23] McQueen, H.J. Met. Forum, 4 (1980) 81-91.
[24] McQueen, H.J. and K. Conrod. In H.J. McQueen et al. (Eds.), *Microstructural Control in Al Alloy Processing.* AIME, Warrendale. 1986, pp. 197-219.
[25] Conrod, K. and H.J. McQueen. In E.A. Starke et al. (Eds.), *Aluminum Alloys. Physical and Mechanical Properties.* Eng. Mat. Advisory Service, Warley, U.K. 1986, pp. 435-447.
[26] McQueen, H.J., E.H. Chia and E.A. Starke. In E.A. Chia et al. [Eds), *Microstructural Control During Al-Alloy Processing.* AIME, Warrendale. 1986, pp. 1-18.
[27] McQueen, H.J. In T.R. Langdon et al. (Eds.) *Hot Working of Aluminum Alloys.* TMS, Warrendale, 1991, pp. 31-54.
[28] Szkrumelak I., K. Conrod and H.J. McQueen. Aluminium, 64 (1988), 1151-1156.
[29] Avramovic-Cingara G. and H.J. McQueen. In Y. Kim et al. (Eds.), *Dispersion Strengthening in Al-*

Alloys. AIME, Warrendale. 1988, pp. 437-450.
[30] E. Evangelista, A. Forcellese, F. Gabrielli and P. Mengucci. In T. Langdon et al. (Eds.), *Hot Deformation of Aluminium Alloys*. TMS, Warrendale. 1991, pp. 121-139.
[31] McQueen, H.J. and N. Ryum. Scand. J. Metals, 14 (1985), 183-194.
[32] Knustad, O., H.J. McQueen, N. Ryum and J.K. Solberg. Practical Metallography, 22 (1985), 215-229.
[33] McQueen, H.J., J.K. Solberg, N. Ryum and E. Nes. In E.A. Starke et al. (Eds.), *Aluminum Alloys. Physical and Mechanical Properties*. Eng. Mat. Advisory Service, Warley. 1986, pp. 513-528.
[34] McQueen, H.J., E. Evangelista, J. Bowles and G. Crawford. Met. Sci., 18 (1984) 395-402.
[35] Evangelista, E., E. Bonetti, E. Di Russo, P. Fiorini and H.J. McQueen. In T. Sheppard (Ed.), *Aluminium Technology '86*. The Metals Society, London. 1986, pp. 185-189.
[36] Evangelista, E., P. Mengucci, E. Di Russo, P. Fiorini and H.J. McQueen. Proc. 8th Light Metal Conference, Leoben. 1987, pp. 544-548.
[37] Evangelista, E., F. Gabrielli, P. Mengucci and E. Quadrini. In P.O. Kettunen et al. (Eds.), *Strength on Metals and alloys*, ICSMA8. Pergamon Press, Oxford. 1988, pp. 977-982.
[38] Evangelista, E., F. Gabrielli, P. Mengucci, E. Quadrini and G. Angioni. *Innovation for Quality*. AIM, Milan. 1988, pp. 205-214.
[39] Evangelista, E., A. Forcellese, F. Gabrielli and P. Mengucci. J. Mat. Proc. Techn., 24 (1990), pp. 323-332.
[40] Verlinden, B., P. Wouters, H.J. McQueen, E. Aernoudt, L. Delaey and S. Cauwenberg. *Mat. Sci. Eng.*, A123 (1990), pp. 229-237; 239-245.
[41] Sankar, J., D. Hawkins and H.J. McQueen. Metals Techn., 6, (1979), 325-331.
[42] Ryan, N.D. and H.J. McQueen. J. Mech. Work. Tech., 12, (1986), 279-286; 323-349.
[43] Luton, M.J. and C.M. Sellars. Acta Metal., 17 (1969), 1033-1043.
[44] Ryan, N.D., H.J. McQueen and J.J. Jonas. Can. Metal. Q., 22 (1983), 369-378.
[45] Ryan, N.D. and H.J. McQueen. Proc. 4th Intnl. Steel Rolling Conf., 1987, pp. F. 17.1-F.17.9.
[46] Fritzmeier, L., M.J. Luton and H.J. McQueen. In P. Haasen (Ed.), *Strength of Metals and Alloys*, ICSMA 5. Pergamon Press, Oxford. 1979, pp. 95-100.
[47] McQueen, H.J., R.A. Petkovic, H. Weiss and L.G. Hinton. In J.B. Ballance (Ed.), *Hot Deformation of Austenite*. AIME, Warrendale. 1977, pp. 113-139.
[48] Weiss, H., D.H. Skinner and J.R. Everett. J. Phys. E, Sci. Instr., 6 (1973), 709-714.
[49] Verlinden, *B. A.T.B.* Metallurgie, 29 [3-4] (1989), 39-48.
[50] Tegart, W.J. McG. and A. Gittins. In J.B. Ballance (Ed.), *Hot Deformation of Austenite*. AIME, Warrendale. 1977, pp. 113-139.
[51] Ahlbom, B. and R. Sandstrom. Int. Met. Rev. 17 (1982), 1-27.
[52] Cingara, A., L. St. Germaine and H.J. McQueen. In A. De Ardo (Ed.), *Processing, Microstructure and Properties of HSLA Steels*. AIME, Warrendale. 1988, pp. 91-114.
[53] McQueen, H.J., A. Cingara, and N.D. Ryan. High Temp. Techn., 9 (1991, in press).
[54] Sheppard, T., S.J. Paterson and M.G. Tutcher. In E.H. Chia et al. (Eds.), *Microstructural Control in Al Alloys*. AIME, Warrendale. 1986, pp. 123-154.
[55] Sheppard, T. and E.P. Wood. Met. Techn., 7 (1980), 58-66.
[56] Sheppard, T., P.J. Tunnicliffe and S.J. Paterson. J. Mech. Work.-Tech., 6 (1982), 313-331.
[57] Sheppard, T. and R.P. Vierod. Mat. Sci. Tech., 1 (1987), 285-290.
[58] Cotner, J.R. and W.J. McG. Tegart. J. Ins. Met., 97 (1969), 73-79.
[59] Kassner, M.E., M.M. Myshlyaev and H.J. McQueen, Mat. Sci. Eng., A108 (1989), 45-61.
[60] McQueen, H.J., J. Sankar and S. Fulop. *Mechanical Behavior of Materials ICM 3*. Pergamon Press, Oxford. 1979, pp. 675-684.
[61] Gittins, A. Metals Forum, 2 (1979), 98-107.

[62] McQueen, H.J., J. Bowles and N.D. Ryan. Microstruct. Sci., 16 (1988), 458-473.
[63] McQueen, H.J. Defects Fracture and Fatigue. M. Nijhoff Pub. The Hague, 1983. pp. 459-471.
[64] McQueen, H.J. and N.D. Ryan. *Stainless Steels '87*. Inst. Metals, London. 1985, pp. 50-61.
[65] Young, C.M. and O. Sherby. *Metal Forming*. Plenum Press, London. 1971, pp. 429-451.
[66] McQueen, H.J., J.K. Solberg, N. Ryum and E. Nes. Phil. Mag., 60 (1989), 473-485.
[67] McQueen, H.J., O. Knustad, N. Ryum and J.K. Solberg. Scripta Met., 19 (1985), 73-78.
[68] Solberg, J.K., H.J. McQueen, N. Ryum and E. Nes. Phil. Mag., 60 (1989), 447-471.
[69] Evangelista, E., H.J. McQueen and E. Bonetti. In J. Bilde-Sorensen et al. (Eds.), *Deformation of Multiphase and Particles containing Materials*. Roskilde. 1983, pp. 243-250.
[70] McQueen, H.J. and W.B. Hutchinson. In N. Hansen et al. (Eds.), *Deformation of Polycrystals*. Roskilde. 1981, pp. 335-342.
[71] Perdrix, C., M.Y. Perrin and F. Montheillet. Mem. Et. Sci. Rev.-Mét., 78 (1981), 309-320.
[72] Montheillet F. *Les Traitments Thérmoméchanique*. P. Costa ed. INSTN, Saclay. 1981, pp. 57-70.
[73] McQueen, H.J. and H. Mecking. Z. Metallkde, 78 (1987), 387-396.73.
[74] McQueen, H.J. Can. Metall. Q. 21, (1982), 445-460.
[75] McQueen, H.J., M.G. Akben and J.J. Jonas. In N.H. Anderson et al. (Eds.), *Microstructural Characterization by Non-Microscopic Techniques*. Riso Ntnl. Laboratory, Roskilde, 1984, pp. 397-403.
[76] Ryan, N.D. and H.J. McQueen. Mat. Forum, 14 (1991, in press).
[77] Ryan, N.D. and H.J. McQueen. Mat. Sci. Tech. (1991, in press).
[78] Ryan, N.D. and H.J. McQeen. Can. Metall. Q. 30 (1991, in press).
[79] McQueen, H.J., E. Fry and N.D. Ryan. *Mathematical Modelling of Hot Rolling of Steel*. S. Yue ed. Can. Inst. Min. Met. Montreal, 1990, pp. 269-280.
[80] Evangelista, E., H.J. McQueen and N.D. Ryan. *Stainless Steels 91*, Iron Steel Inst. Japan, 1991, in pp. 842-849.
[81] Streisselberger, A., R. Kaspar and O. Pawelski. Metall. Trans., 16A, (1985), 67-72.
[82] McQueen, H.J., E. Evangelista and N.D. Ryan. *Innovation for Quality*. AIM Milano, 1988, pp. 212-220.
[83] McQueen, H.J., G. Avamovic-Cingara. A. Salama and T.R. McNelley. Scripta Met., 23 (1989), 273-278.
[84] McQueen, H.J. Jour. Met., 32, (1980) 17-36.
[85] McQueen, H.J. and J.J. Jonas. In C.Q. Chen et al. (Eds.), *Aluminium Alloys 90 (ICAA 2;* C.Q. Chenetal Intnl. (Eds.) Academic Pub. Beijng 1990, pp. 727-742.
[86] Smith, I.C., G. Avramovic-Cingara and H.J. McQueen. In Y.H. Sanders et al. (Eds.), *Aluminium Lithium Alloys. V.* MCPE Publications, Birmingham, 1989, pp. 223-232.
[87] Avramovic-Cingara, G. and H.J. McQueen. *Advanced Aluminium and Magnesium Alloys*. ASM International, Materials Park, 1991, in press.

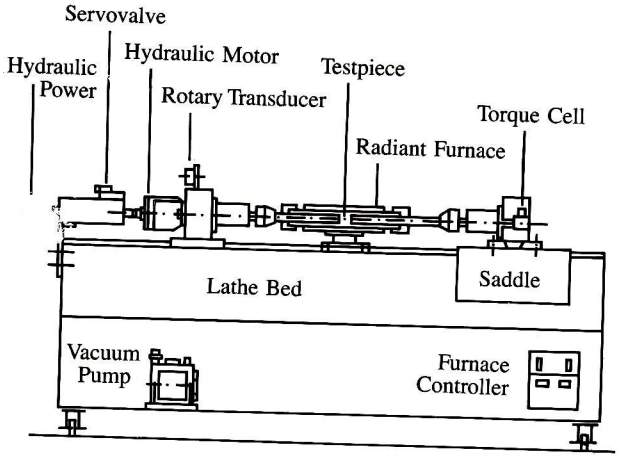

Fig. 1:
The servo-controlled hydraulic torsion machine with the major components indicated.

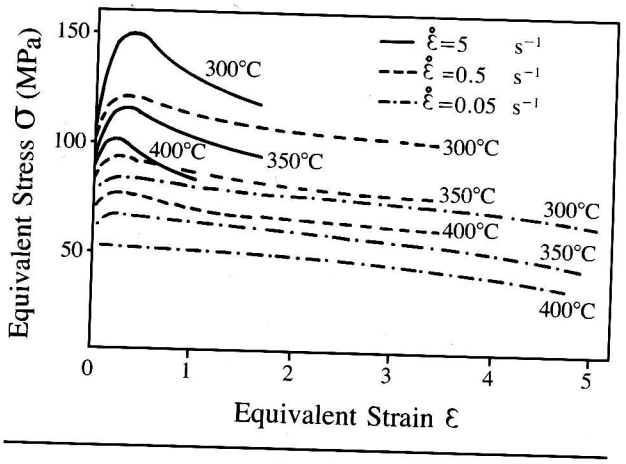

Fig. 2:
Typical stress-strain curves for AA7012 Al alloy after precipitation treatments at different temperatures and strain rates [36].

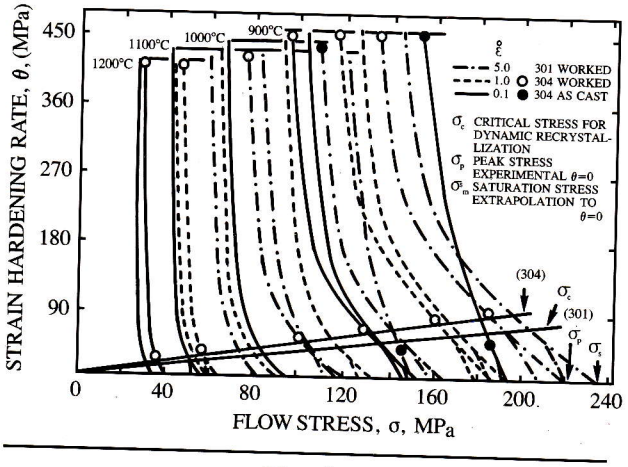

Fig. 3:
Plots of Θ vs σ for AISI 301 and 304 stainless steels exhibit increased dynamic recovered by shifting downward to the left as temperature rises and strain rate decreases. Higher levels of DRV at higher T and lower ε give rise to curves closer to the origin [12].

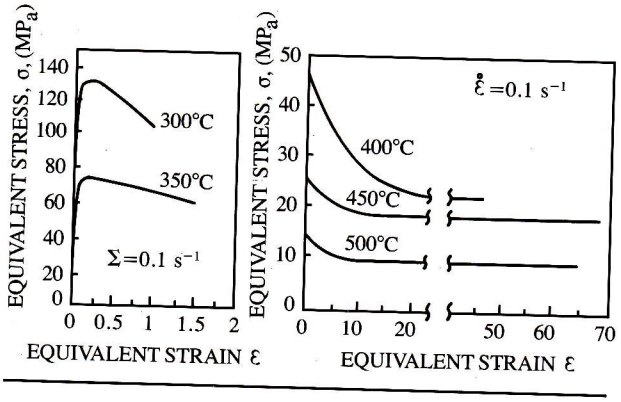

Fig. 4:
Equivalent stress-strain curves of solution treated AA6015 Al alloy; the precipitation occurs during deformation [39].

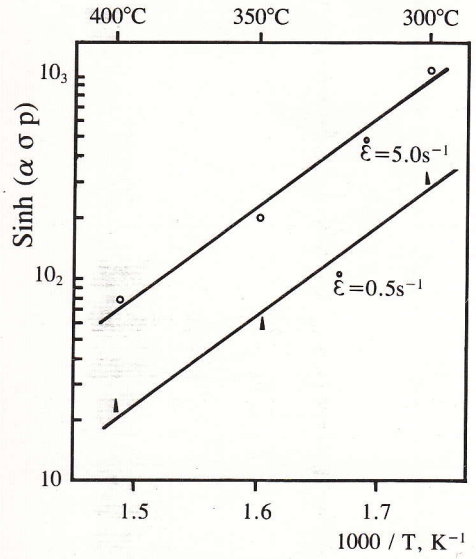

Fig. 5:
Dependence of sinh ($\alpha\ \sigma_p$), at constant $\dot{\varepsilon}$, on temperature in AA7012. The slope gives an activation energy of 145 kJ/mol [35].

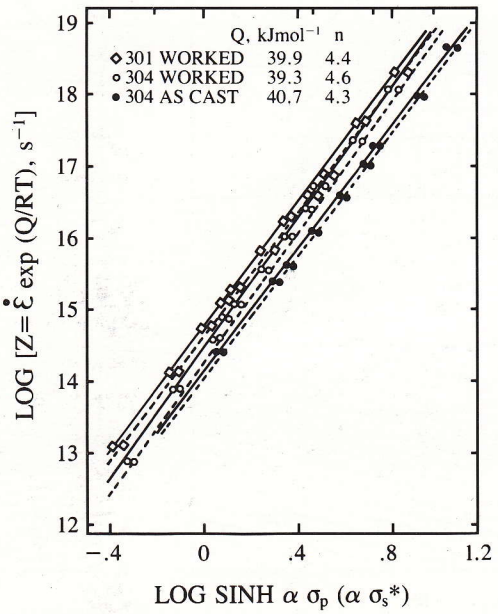

Fig. 6:
The variation of σ_p, peak flow stress (——), and σ_s*, saturation test (— — —), for as cast 304 and for worked-homogenized 304 and 301 steels [10].

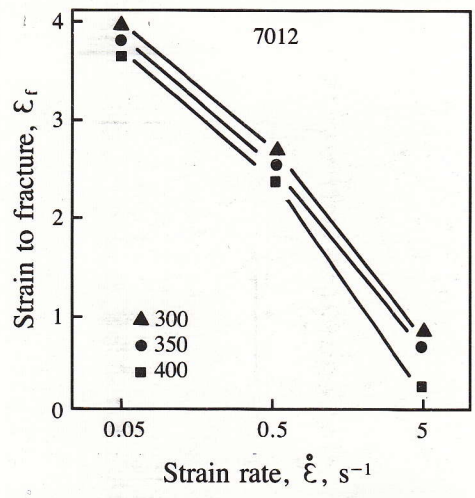

Fig. 7:
Hot ductility trends expressed as equivalent strain to fracture for AA7012 alloy after precipitation treatments. Like in fig. 2, ε_f decreases as T rises because solute enrichment as precipitates partially dissolve.

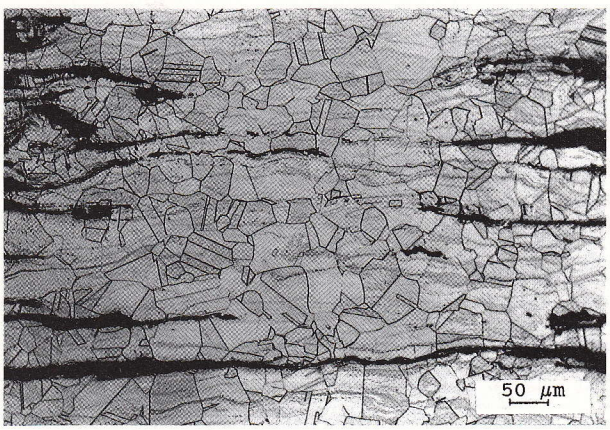

Fig. 8:
Tangential section of 301W tested at 1100°C and 5 s^{-1}. Broad surface cracks are marked at opposite edges where the section is close to the surface and almost disappear in the middle, except for their deepest tips.

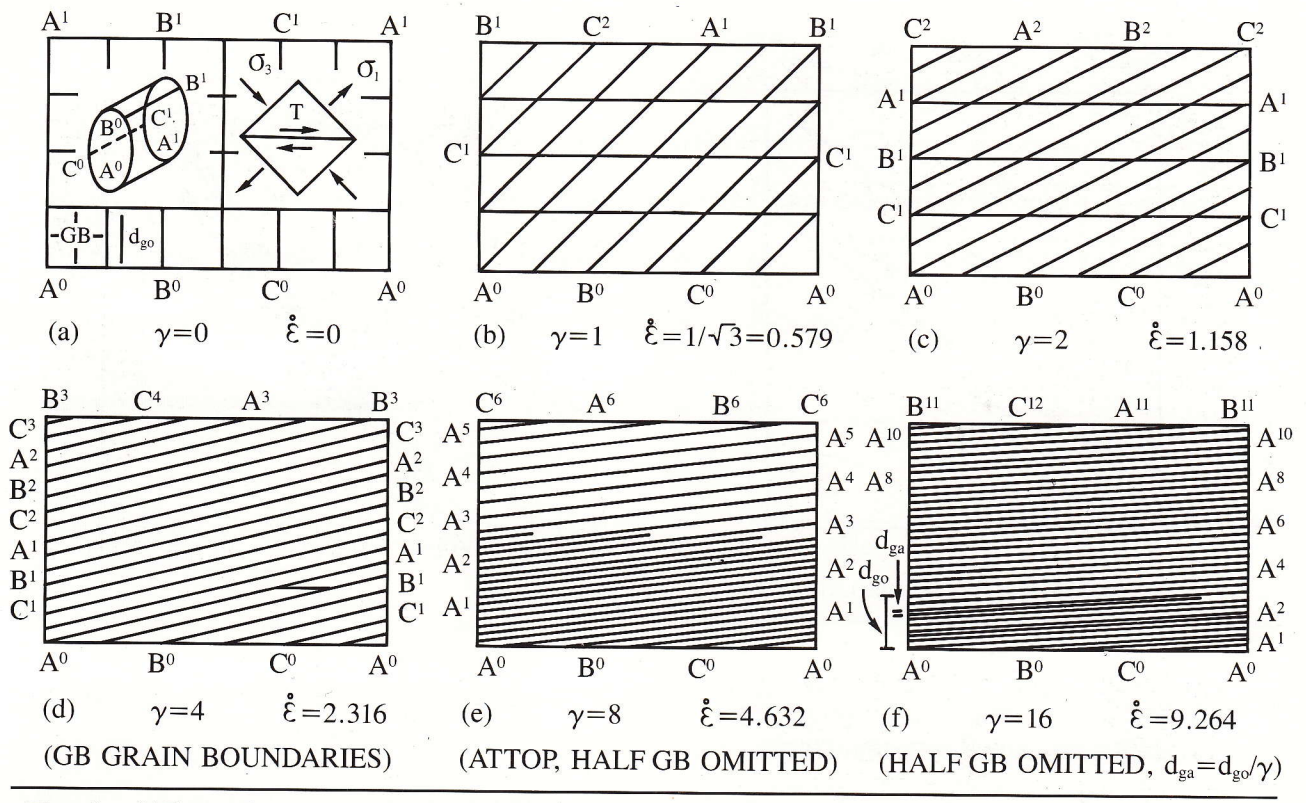

Fig. 9: a) The surface of a torsion specimen is slit and unfolded into a rectangle $A^\circ A^\circ A^1 A^1$ and divided into squares of edge d_{go}. The primary stress cube, $\sigma_2 = 0$ is normal to the paper. The strain is incresed to $\gamma = 1$ in (b) and then progressively doubled. The grains are seen to become progressively thinner $d_g \approx d_{go}/\gamma$ and at higher angle to axis. The radial dimension remains constant. One grain is outlined.

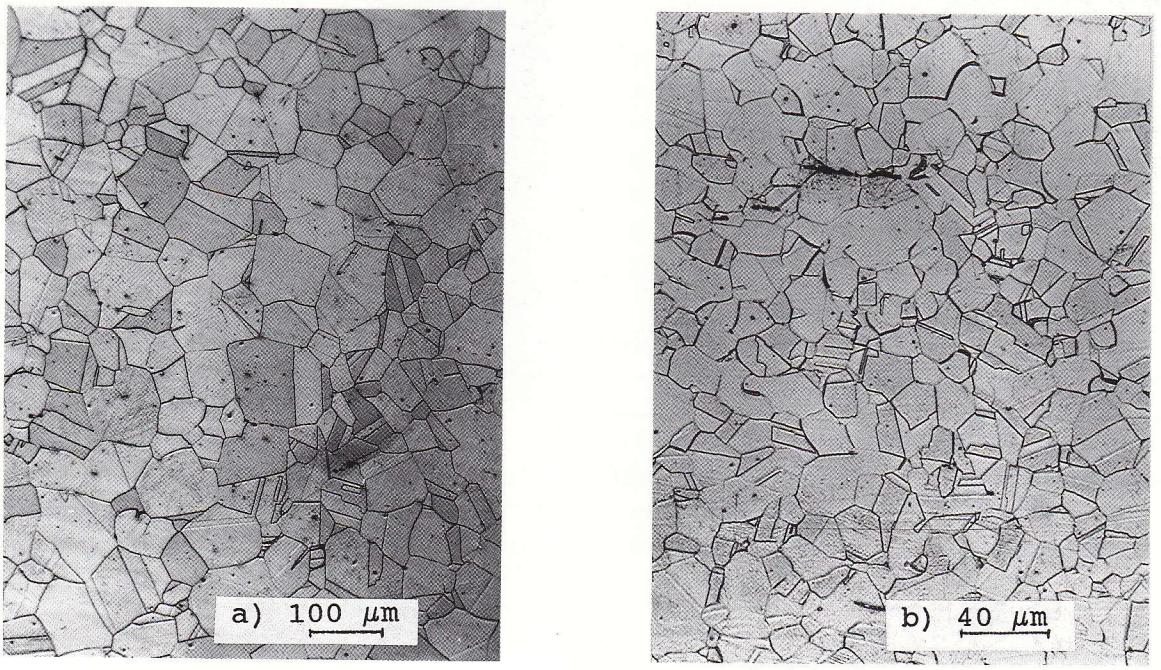

a) prior to hot torsion;

b) deformed at 1000°C, 5 s^{-1} showing refined DRX grains.

Fig. 10:
Microstructure of tangential sections of 316.

Fig. 11:
TEM micrographs showing the effect of rising T at 5 s^{-1} on subgrain size d_s of AISI 316 a) 900°C, b) 1000°C, c) 1100°C.

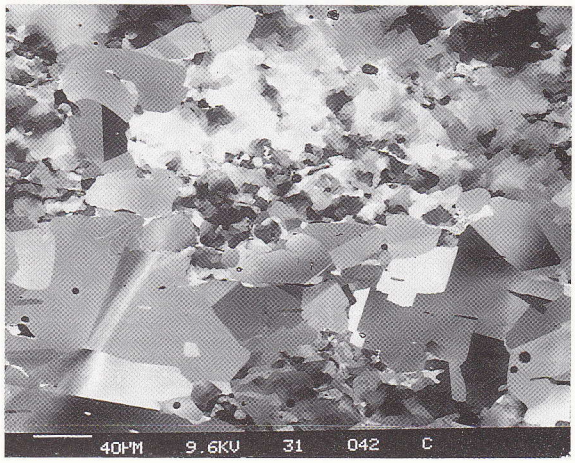

Fig. 12:
Microstructures, by SEM channeling contrast, of 317C torsioned beyond the peak at 1100°C, 0.1 s^{-1} showing some elongated δ particles, worked regions with small subgrains and SRX grains [13-15].

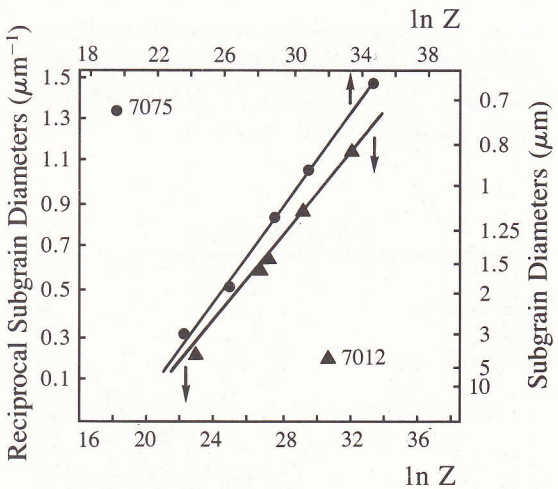

Fig. 13:
Diameter variation of subgrains in AA7012 and AA7075 after precipitation treatmens as function of Z parameter [36].

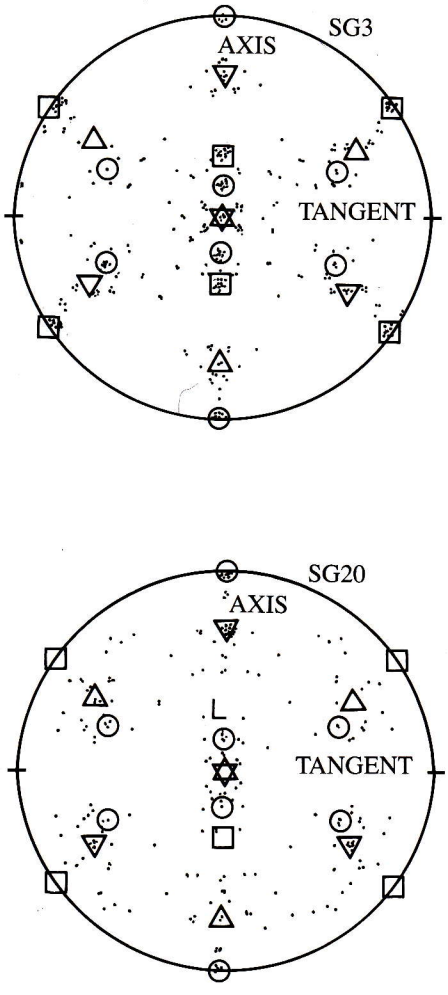

Fig. 14:
{111} pole figures derived from SEM channeling patterns on tangential fine grained flat specimens of Al 99.9 deformed to a) $\varepsilon = 3$; mixtures of ideal orientation (112) [110] {111} and (110) [110] {001}; b) $\varepsilon = 20$, major ideal orientation (111) [110] {112}.

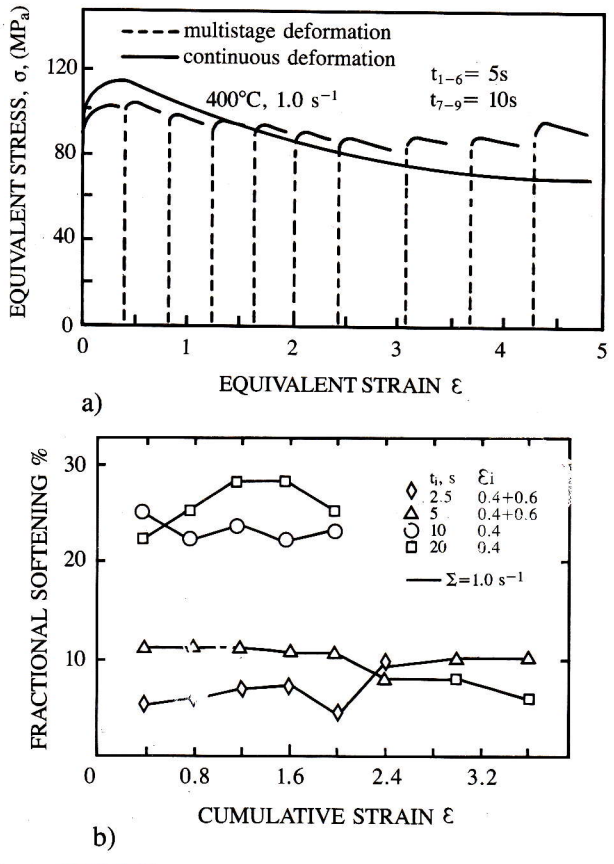

Fig. 15:
a) Multistage isothermal flow curves for AA5083 at 400°C and 1.0 s^{-1} and b) the derived fractional softening [34,69].

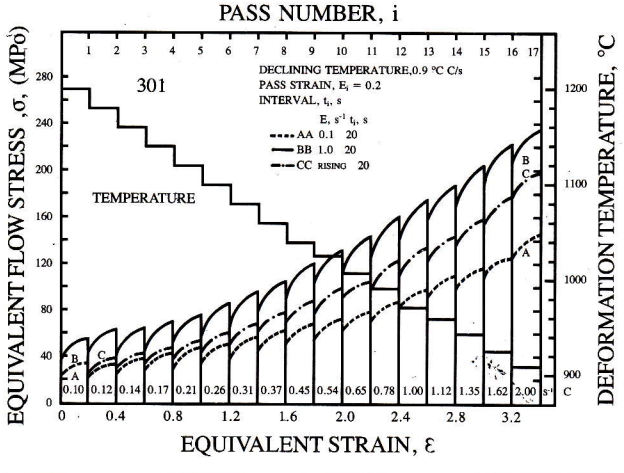

Fig. 16:
Multistage deformation of 301W for declining T of 0.9°C/s (1200-900°C); $\varepsilon = 0.1$ (AA) or 1.0 s^{-1} (BB) or rises gradually from 0.1 to 2.0 s^{-1} (CC).

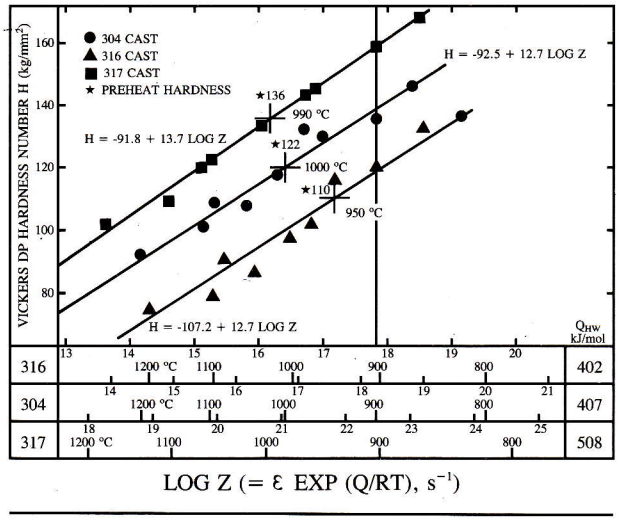

Fig. 17:
Hardness for 304 C, 316 C and 317 C is uniquely dependent on Z and is strongly affected by volume fraction of δ particles [78].